Physics – Uspekhi **50** (10) 1079 – 1082 (2007)

METHODOLOGICAL NOTES PACS numbers: **79.60.–i**, 79.60.Dp

Tunneling photoeffect mechanism in metallic nanoparticles activated by cesium and oxygen

É L Nolle

DOI: 10.1070/PU2007v050n10ABEH006368

Contents

Abstract. The long-wavelength surface-plasmon-induced portion of the photoelectron emission (PE) spectrum of granulated silver and gold films activated by cesium and oxygen is found to shift toward the short-wavelength region with respect to the optical absorption band. The intensity of this long-wavelength portion decreases exponentially with increasing wavelength, and a photoelectric threshold is not detected. The photoeffect in such structures is shown to be determined by the probability of tunneling nonequilibrium photoelectrons through the potential barrier formed by an activating layer. The PE spectra calculated in the triangle barrier approximation agree well with appropriate experimental spectra.

1. Introduction

The tunneling mechanism of electron transitions is the basis for many physical processes in solids. In some cases, it manifests itself when an electric field is applied, for example, during the field electron emission considered by Fowler and Nordheim [1] or during light absorption in semiconductors (Franz – Keldysh effect) [2]. In the course of field emission, equilibrium electrons tunnel from the Fermi level in a solid into a vacuum. In this case, the emission current is specified by the electron tunneling probability from the solid surface through a potential barrier whose shape is close to a triangle, and this current increases exponentially with the applied field strength F. In the Franz – Keldysh effect, the light quantum absorption probability for energies $h\nu < E_g$, where E_g is the band gap of a semiconductor, increases with the applied field F. It is impossible to exactly determine E_g, since the light absorption probability at a given value of F decreases exponentially with decreasing energy $h\nu$.

É L Nolle A M Prokhorov General Physics Institute,
Russian Academy of Sciences,
ul. Vavilova 38, 119991 Moscow, Russian Federation
Tel. (7-499) 503 83 23
E-mail: nolle@ran.gpi.ru

Received 12 March 2007, revised 5 June 2007
Uspekhi Fizicheskikh Nauk **177** (10) 1133 – 1137 (2007)
DOI: 10.3367/UFNr.0177.200710d.1133
Translated by K V Shakhlevich; edited by A Radzig

In granulated metallic films, new light absorption bands are known to appear; they are caused by surface-plasmon excitation in the nanoparticles making up these films [3, 4]. For example, absorption bands appear at a wavelength $\lambda \approx 500$ nm in granulated Ag films [3] and are absent in solid films. According to the Mie theory [5], the light absorption cross section of a spherical nanoparticle of volume V for nanoparticles whose linear dimensions are much smaller than λ is given by

$$\sigma(\lambda) = \frac{18\pi V \varepsilon_2(\lambda)}{\lambda\left[(\varepsilon_1(\lambda)+2)^2 + \varepsilon_2^2(\lambda)\right]}\,, \tag{1}$$

where $\varepsilon_1(\lambda) + \mathrm{i}\varepsilon_2(\lambda) = \varepsilon(\lambda)$ is the dielectric constant of the metal, and a surface plasma resonance occurs at λ_p, where $\varepsilon_1(\lambda_p) = -2$. In spheroidal nanoparticles, this resonance shifts toward long wavelengths with respect to the resonance in spherical nanoparticles. This shift increases as the spheroid axial ratio $R = b/a$ decreases. Nanoparticles produced by various methods — thermal or laser deposition, chemical vapor deposition, etc. — are always characterized by a spread in R. Therefore, their shape can be close to a sphere; then, the average value of R exceeds 0.5, and surface-plasmon absorption is maximal [see Eqn (1)] near λ_p, where $\varepsilon_1(\lambda_p) = -2$. Moreover, nanoparticles can have the shape of an oblate or prolate spheroid; in this case, $R \ll 1$, and the surface-plasmon absorption maximum shifts strongly toward long wavelengths with respect to λ_p and is located near $\lambda_{max} \approx 2\lambda_p/\sqrt{\pi R}$. According to Ref. [3], the spectral dependence of the light absorption coefficient for spheroids with different values of R represents the envelope of the Gaussian distribution of the absorption cross sections for these nanoparticles and can be written out as

$$\alpha(\lambda) = \frac{N}{\sigma_\eta\sqrt{2\pi}} \int_0^\infty \sigma(\lambda,\eta) \exp\left[-\frac{(\eta-\eta_0)^2}{2\sigma_\eta^2}\right] \mathrm{d}\eta\,, \tag{2}$$

where N is the number of nanoparticles on the surface; $R = \eta/\sqrt{1+\eta^2}$; η_0 is the average value equal to b/c for $b/a \ll 1$, and σ_η is the standard deviation of the Gaussian distribution.

In Refs [6, 7], we detected photoelectron emission induced by surface-plasmon excitation in the visible region from Ag

and Au nanoparticles whose surface was activated by cesium and oxygen. The properties of plasmons in the visible region were studied previously in numerous works using light absorption. In these works, opaque substrates were utilized; therefore, absorption spectra could not be recorded. For studying the properties of thin films, photoelectron emission (PE) is much more sensitive than optical absorption. As follows from Refs [6, 7], the PE spectra of the activated Ag and Au nanoparticles possess no distinct photoemission threshold $\lambda_0 = c/\nu_0$. The purpose of this work is to study simultaneously the PE and optical absorption spectra of the activated Ag and Au nanoparticles with the goal of determining the cause of the absence of a distinct photoelectric threshold in such structures and revealing the photoeffect mechanism in them.

2. Arrangement of the experiment. Results and discussion

We fabricated Ag and Au granulated films, activated them by Cs and O, measured their PE and absorption spectra, and determined their surface composition by X-ray photoelectron spectroscopy (XPES) at a pressure of 10^{-10} Torr. All measurements were performed at room temperature. A thin Ag or Au film was evaporated onto a 20-nm-thick InO_2–SnO_2 transparent and conducting film supported on a glass substrate. The average thickness of the former film was 4–5 nm, as determined by a quartz weight meter. A substrate coated with a metallic film was heated at 300 °C for 20 min. Under these conditions, the granulated Ag films consist of oblate spheroids [3], and the deposited Au films consist of nanoparticles whose shape is close to a sphere [4]. The formation of Ag and Au nanoparticles in our work was corroborated by XPES data. Thermally evaporated metallic films with an average thickness of less than 10 nm are typically known to be discontinuous and nonconducting. Therefore, apart from Ag($3d_5$) and Au($4f_7$) peaks, the XPES spectra of the evaporated gold and silver films also contained In($3d_5$), Sn($3d_5$), and O(1s) peaks possessed by the substrate. For a 4- to 5-nm thick continuous film, no peaks from substrate elements should appear due to a small photoelectron escape depth in XPES, which is about 1 nm. After sample heating, the substrate peaks increased sharply and the Ag and Au peak intensities simultaneously decreased. This change in the XPES peaks is caused by a decrease in the substrate surface covered by an evaporated metal upon heating, which corresponds to the formation of metallic nanoparticles. The granulated Ag and Au films were activated by the traditional technique of activating semiconductor photocathodes with a negative electron affinity [8]. This activation technique leads to a higher photoelectron escape probability into a vacuum as compared to the activation by only Cs, which allowed us to generate intense PE induced by surface-plasmon excitation in Ag and Au nanoparticles in the visible region [6, 7]. While earlier, PE from metallic films has been detected only in the UV region.

For Au nanoparticles, the light absorption $\alpha(\lambda)/\alpha_{max}$ and PE quantum yield $Q(\lambda)/Q_{max}$ maxima were located near the maximum calculated from Eqn (1), which indicates that the shape of the Au nanoparticles was close to a sphere. The width of absorption spectrum in this case is significantly larger than the width determined by Eqn (1) and corresponds to Gaussian distribution (2) with the parameters $R = 0.65$ and $\sigma_\eta = 0.3$. The XPES study of the ratio between free

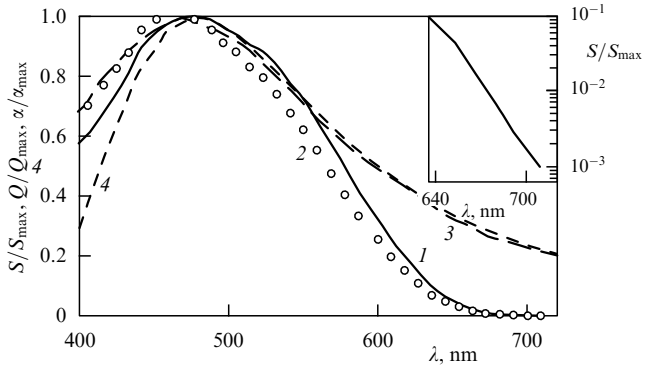

Figure 1. Ag nanoparticle spectra: (*1*) sensitivity S/S_{max}, (*2*) quantum yield Q/Q_{max}, (*3*) experimental absorption α/α_{max}, and (*4*) absorption calculated by Eqn (2). The inset shows the long-wavelength portion of the S/S_{max} spectrum.

substrate surface area and area covered by gold after heating demonstrates that, in the case of quasispherical ($R = 0.65$) nanoparticles, their radius reaches 4–6 nm and the light absorption spectrum is specified by surface-plasmon excitation in these nanoparticles. The light absorption spectrum of the Ag nanoparticles (Fig. 1, curve *3*) coincided with the spectrum calculated by Eqn (2) at $\sigma_\eta = 0.045$ and $\eta_0 = 0.1$ (Fig. 1, curve *4*). This corresponds to a plasma resonance for oblate spheroids with an axial ratio $b/a \approx 0.1$ and, according to Ref. [3], $a \approx 50$ nm. As follows from Eqn (1), the surface plasmon resonance for spherical Ag nanoparticles is maximal at $\lambda_p \approx 350$ nm, and it was not studied in this work. The PE spectra of none of the Ag and Au samples had a clear photoelectric threshold. The sensitivity in the long-wavelength region of the PE spectra decreased exponentially to S with increasing wavelength λ, which is specified by the sensitivity limit of the available apparatus (inset to Fig. 1a).

Another specific feature of the Ag and Au samples is a shift in the long-wavelength region of the PE spectra toward the short-wavelength region with respect to the long-wavelength region of the absorption spectra (Fig. 1, curves *1–3*). Figure 2 depicts the long-wavelength portions of the quantum yield (Q/Q_{max}) and light absorption (α/α_{max}) spectra as a function of the photon energy $h\nu$ for Ag

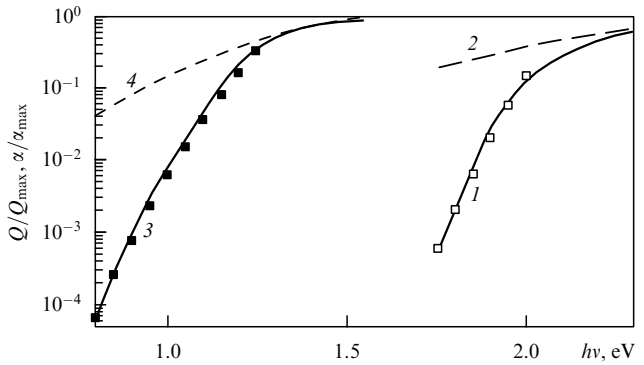

Figure 2. Quantum yield Q/Q_{max} (*1*) and absorption α/α_{max} (*2*) spectra of Ag nanoparticles after optimum activation. Quantum yield Q/Q_{max} spectrum (*3*) and absorption α/α_{max} spectrum (*4*) calculated by Eqn (2) for an S-1 photocathode. Points in the curves are the Q/Q_{max} spectra calculated by Eqn (3) for the barrier parameters given in Table 1.

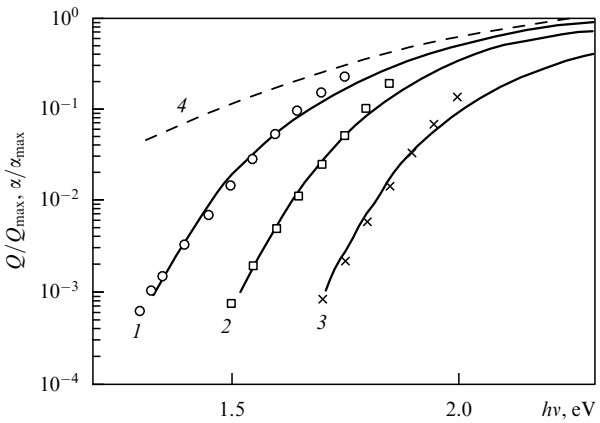

Figure 3. Au nanoparticle spectra of the quantum yield Q/Q_{max} after optimum activation (*1*) and PE degradation (*2*, *3*), and of the absorption spectrum α/α_{max} (*4*). Points in the curves are the Q/Q_{max} spectra calculated by Eqn (3) for the barrier parameters given in Table 1.

nanoparticles (curves *1*, *2*) and the Q/Q_{max} spectrum of a silver–oxygen–cesium S-1 photocathode (Hamamatsu, Japan) (curve *3*).[1] The S-1 photocathode characteristics were approximated using an absorption spectrum calculated by Eqn (2) with the parameters $\sigma_\eta = 0.018$ and $\eta_0 = 0.035$ (curve *4*). As is seen from Fig. 2, the PE and absorption spectra of the S-1 photocathode (curves *3*, *4*) are similar to those of Ag nanoparticles. However, the shift in the spectra of the S-1 photocathode with respect to the spectra of spherical nanoparticles toward low photon energies is larger than that in the spectra of silver nanoparticles (curves *1*, *2*). This shift is explained by the fact that the difference in the ratios of axial lengths for the spheroidal Ag nanoparticles in the S-1 photocathode (for which $\eta_0 = b/a = 0.035$) is significantly larger than those of the Ag nanoparticles ($\eta_0 = 0.1$) produced by thermal evaporation, since the process of S-1 photocathode growing differs substantially from the more simple process of thermal evaporation. Figure 3 displays the Q/Q_{max} PE spectrum of Au nanoparticles as a function of the energy $h\nu$ after optimum activation (curve *1*) and a decrease in the PE intensity of the Au samples (curves *2*, *3* corresponding to PE degradation) upon weak excess Cs adsorption after their activation. In this case, the shift in the PE spectra (curves *2*, *3*) with respect to the light absorption spectrum (curve *4*), which does not change during PE degradation, is even larger. The intensity in the long-wavelength region of the PE spectrum therewith continues to exponentially decrease with increasing wavelength λ, and the spectrum has no step indicating a photoelectric threshold. The short-wavelength portions of the PE and absorption spectra (Fig. 1, curves *1*–*3*) coincided, and the quantum yield (the ratio of the number of photoelectrons to the number of absorbed photons) for the Ag and Au samples was $Q \approx 0.01$.

The absence of a photoelectric threshold, the exponential decrease in the intensity of the long-wavelength portion of the PE spectrum, and its shift toward the short-wavelength region with respect to the light absorption spectrum of activated Ag and Au nanoparticles point to a tunneling photoeffect mechanism in such structures. In this case, photons excite surface plasmons in the nanoparticles, and their absorption

[1] Cat. No. SSC1047E01 MAY/97 CR, printed in Japan (2000).

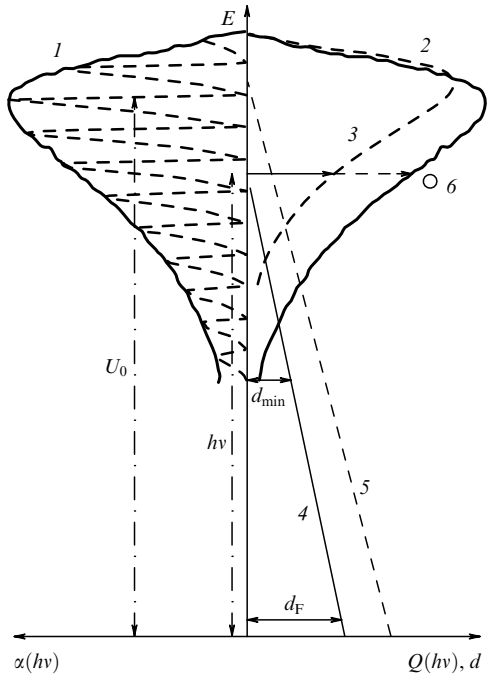

Figure 4. Schematics of the photoeffect in activated nanoparticles: (*1*) envelope of the $\alpha(h\nu)$ absorption spectra for nanoparticles with different b/a ratios, (*2*) envelope of the quantum yield $Q(h\nu)$ spectra for photoelectrons tunneling through the barrier *4* after optimum activation, (*3*) the same for photoelectrons tunneling through the barrier *5* after PE degradation, and (*6*) schematic for the escape of photoelectrons excited by $h\nu$ light quanta after optimum activation and PE degradation, respectively; d_{min} and d_F are the tunneling lengths given in Table 1.

spectrum is described by Eqn (2), as illustrated in Fig. 4 (curve *1*). The dashed lines under solid curve *1* represent the absorption spectra of individual nanoparticles with various axial ratios b/a, which are characterized by a Gaussian distribution. These spectra are obtained from Eqn (2) at $\sigma_\eta = 0$ for the appropriate η_0 parameters which depend on the b/a ratio. A part of plasmons determined by $Q \approx 0.01$ emit electrons into the vacuum, and the remaining plasmons dissipate their energy in nanoparticles or emit light quanta. However, not all of the electrons can escape from the nanoparticle surface into the vacuum. This surface has a potential barrier formed by an activating layer which consists of Cs^+ and $Cs^+ - {}^-O^- - Cs^+$ dipoles [8]. This barrier can be approximated by a triangle. The barrier height U_0 measured from the Fermi level E_F and the field strength F are determined from experiment using the expression

$$\frac{Q(h\nu)}{Q_{max}} = \frac{P(h\nu)\alpha(h\nu)}{\alpha_{max}}\,, \tag{3}$$

where $P(h\nu)$ is the escape probability of an electron with an energy $h\nu$ into a vacuum via tunneling through the barrier

Table 1.

	U_0, eV	F, V cm^{-1}	$h\nu_{min}$, eV	d_{min}, nm	d_F, nm
Au^0	1.85	6.9×10^6	1.3	0.8	2.7
Au^1	2	5×10^6	1.5	1	4
Au^2	2.22	4.7×10^6	1.7	1.1	4.7
Ag	2.33	3.8×10^6	1.75	1.5	6.2
S-1	1.33	4.4×10^6	0.8	1.2	3

with the height U_0 in the field F [9]:

$$P(h\nu) = \exp\left[-\frac{4\sqrt{2m}\,(U_0 - h\nu)^{3/2}}{3\eta F}\right]. \quad (4)$$

The long-wavelength regions of the experimental PE spectra of Ag (Fig. 2, curve *1*) and Au (Fig. 3, curves *1–3*) nanoparticles agree with the values (points in the respective curves) calculated by Eqn (3) for a tunneling photoeffect mechanism. The same agreement (Fig. 2, curve *3*) was obtained for the S-1 photocathode. According to Ref. [6], the photoelectron emission from the S-1 photocathode is caused by surface-plasmon excitation in the Ag nanoparticles of this photocathode. The absence of a photoelectric threshold in its PE spectrum is also related to photoelectron tunneling through an activating Cs–O layer. Table 1 gives the parameters U_0 and F determined from the experimental data using formula (3) for activated silver and gold nanoparticles (Au^0, after optimum activation; Au^1 and Au^2, after PE degradation) and for the S-1 photocathode. The table also presents the photoelectron tunneling lengths $d_{\min}$ for the values of $h\nu_{\min}$ specified by the thresholds of sensitivity of the available apparatus, as well as the electron tunneling lengths d_F from the Fermi level at the appropriate values of U_0 and F. Apparently, these lengths should be smaller than the activating layer thickness which is about 1 nm and 10 nm in dipole and heterojunction models, respectively, for a decrease in the vacuum level [8]. As follows from the table, the experimental values of $d_{\min}$ fit into the dipole model, and the values of d_F into the heterojunction model. This raises the question of whether a photoelectric threshold exists in the activated metallic nanoparticles. If this threshold does not exist and the vacuum level coincides with the Fermi level in a nanoparticle, the escape probability of photoelectrons with an energy close to kT for the S-1 photocathode is on the order of $P \approx 10^{-11}$ for the triangle barrier approximation with the parameters (see Table 1) corresponding to the energy range $h\nu = 0.8-1.2$ eV (see Fig. 2, curve *3*).

The agreement between the PE spectra calculated by formula (3) and the experimental spectra indicates that the photoeffect in the metallic nanoparticles activated by cesium and oxygen is caused by photoelectron tunneling through the potential barrier formed by the activating layer. In this case, the photoeffect is characterized by nonequilibrium-photoelectron tunneling probability $P(h\nu)$ which depends on the energy $h\nu$ of photons exciting photoelectrons. The $P(h\nu)$ probability depends on the potential-barrier height, width, and shape. For the triangle barrier approximation, the $P(h\nu)$ probability is described by formula (4) and depends on the electric field strength F in the activating layer and the barrier height U_0 at the metal–activating layer interface. The value of U_0 when $F \to 0$ can be considered as a work function φ of electrons. In this case, the potential barrier transforms into a potential wall of height φ. As in many works dealing with the S-1 photocathode, we did not reveal a photoelectric threshold, which determines the work function from the surface of activated Ag and Au nanoparticles, in this work. The PE spectra of these structures in the photon energy range under study are determined by the escape probability $P(h\nu)$. A similar PE mechanism was observed in gallium arsenide activated by Cs and O [10]; in GaAs, however, quasiequilibrium photoelectrons tunneling occurred from the γ and L subbands of the conduction band. Therefore, the photoelectron escape probability in Ref. [10] was independent of $h\nu$ and was determined by the subband energies E_γ and E_L, while the photoelectric threshold was specified by the band gap in GaAs.

According to the PE model proposed, an increase in the photoelectron escape probability upon activation or a decrease upon PE degradation is caused by a change in the potential-barrier parameters rather than a decrease or increase in the potential-wall height (a decrease or an increase in φ, respectively). Such changes in the barrier parameters upon PE degradation in the Au samples are seen from Fig. 3 (curves *2*, *3*) and the table, as well as from the Cs and O activation of gallium arsenide in Ref. [10]. Therefore, the photoelectron escape probability from the surface of an activated photoemitter can vary with $h\nu$ from 1 to 0 rather than as $P = 1$ for $h\nu > h\nu_0$ and $P = 0$ for $h\nu < h\nu_0$, as was generally accepted.

3. Conclusion

We qualitatively grounded the agreement between experimental data and a proposed tunneling photoeffect mechanism in metallic nanoparticles activated by Cs and O. As a result, we were able to explain the specific features in the PE spectra of such structures and the absence of a photoelectric threshold in them. In this connection it is necessary to microscopically consider the potential-barrier parameters in the activating layer and to investigate the interaction of the layer dipoles with the dipole moments of the excited nanoparticles.

References

1. Fowler R H, Nordheim L *Proc. R. Soc. London Ser. A* **119** 173 (1928)
2. Keldysh L V *Zh. Eksp. Teor. Fiz.* **34** 1138 (1958) [*Sov. Phys. JETP* **7** 788 (1958)]
3. Kennerly S W et al. *Phys. Rev. B* **29** 2926 (1984)
4. Grandqvist C G *Phys. Rev. B* **16** 3513 (1977)
5. Kerker M *The Scattering of Light, and Other Electromagnetic Radiation* (New York: Academic Press, 1969)
6. Nolle É L, Schelev M Ya *Pis'ma Zh. Tekh. Fiz.* **30** (8) 1 (2004) [*Tech. Phys. Lett.* **30** 304 (2004)]
7. Nolle É L, Schelev M Ya *Zh. Tekh. Fiz.* **75** (11) 136 (2005) [*Tech. Phys.* **50** 1528 (2005)]
8. Bell R L *Negative Affinity Devices* (Oxford: Clarendon Press, 1973)
9. Landau L D, Lifshitz E M *Kvantovaya Mekhanika* (Quantum Mechanics: Non-Relativistic Theory) (Moscow: Fizmatgiz, 1963) [Translated into English (Oxford: Pergamon Press, 1965)]
10. Nolle É L *Fiz. Tverd. Tela* **31** 225 (1989) [*Solid State Phys.* **31** 196 (1989)]